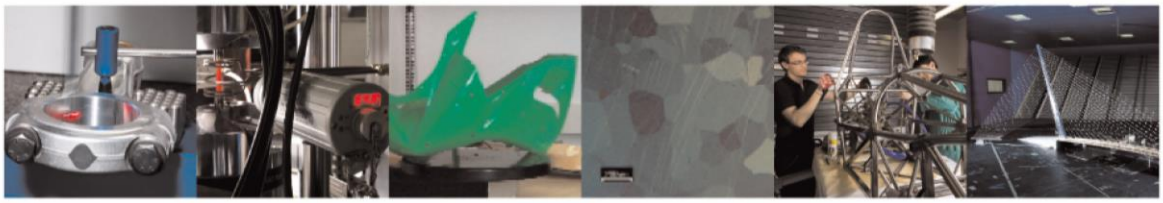

Prototyping of biodegradable flat stents in pure zinc by laser microcutting and chemical etching

Catalano, Guendalina; Demir, Ali Gökhan; Furlan, Valentina; Previtali, Barbara

DIPARTIMENTO DI MECCANICA ■ POLITECNICO DI MILANO
via G. La Masa, 1 ■ 20156 Milano ■ EMAIL (PEC): pecmecc@cert.polimi.it
http://www.mecc.polimi.it
Rev. 0

Prototyping of biodegradable flat stents in pure zinc by laser microcutting and chemical etching

Guendalina Catalano[a], Ali Gökhan Demir[a,*], Valentina Furlan[a], Barbara Previtali[a]

[a]*Department of Mechanical Engineering, Politecnico di Milano, Via La Masa 1, 20156 Milan, Italy*

*Corresponding author: aligokhan.demir@polimi.it

Abstract

Cardiovascular stents are biomedical devices, which restore normal blood flow in the case of coronary artery obstructions. Biodegradable metals provide the possibility of a less-invasive treatment, where the stent is dissolved in body fluids after the remodelling of the artery. Compared to Mg- and Fe-alloys, Zn and its alloys provide optimal corrosion rates as a more recent option. New Zn-alloys are under development and often need to be tested for corrosion and biological properties. However, Zn and its alloys still require further investigation in terms of the production routes involved for the stent manufacturing. Especially at a prototyping stage, extrusion of thin biodegradable tubes is an expensive and difficult process. This work investigates a novel manufacturing route consisting in laser microcutting and chemical etching of pure Zn sheets to develop inflatable devices that can take a tubular form. Initially, laser microcutting parameters were studied to understand the dross formation on a low melting point material. Chemical etching of the material with low corrosion resistance was investigated for the dross removal. Prototype flat stents were produced and expanded using a medical catheter.

Keywords: Cardiovascular stent, sheet metal, pure zinc, biodegradability, laser microcutting, chemical etching.

1. Introduction

The use of cardiovascular stent is the common practice for the treatment of stenosis. Material and stents design are the crucial aspects of the functioning of the device [1] Stents can be divided in permanent and biodegradable devices and has to maintain mechanical integrity during its insertion, expansion, and until the remodelling of the vessel is completed [2]. Moreover, permanent stents present problem infant patients, because the arteries have to grow in time. In this condition, the risk of implant movement inside the vessel is high. In order to avoid these problems and inflammations reactions it has been proposed to produce stents in biodegradable materials, where biodegradable is the device ability to be dissolve by human fluids. The selection of biodegradable alloy is not a simple issue. The concept of a biodegradable device becomes of great interest at this point, where the presence of the stent is unnecessary, and can also increase the risk of restenosis [3]. In particular, the attention is focalized on materials which are already present in human body and which

are biocompatible with this one. Biodegradable device should be characterized by a defined time of mechanical integrity, which should be followed by a correct stent degradation [4]. In this perspective, the selection of elements like magnesium, pure iron and their alloys as biodegradable materials is in accordance with defined requirements. Magnesium, for example is a deeply investigated biodegradable metallic material, which is involved in biomedical stent research [4]–[11]. Magnesium represents a great innovation for the realization of biodegradable stents, however is characterised by high degradation rates human body [6], [7], [9], [12], [13]. Magnesium has excessive speed of degradation in a physiological environment characterized by pH about 7.4-7.6, and within a blood vessel is completely corroded in 12- 14 weeks, invalidating the obtainment of the desired result, according to which the stent length should be about 8-10 months [13]. Another option, as employed degradable material, is related Fe-alloys [4], [14], [15]. The main drawback is the low biodegradation rate, which limits their applicability in cardiovascular stents. More recently, the concept of Zinc as an option for stent fabrication started from its firstly employment [3], [16]–[18]. Zn participates in basic biological functions. It is an antioxidant and an endothelial membrane stabilizer. The maximum daily intake of Zn is 10 mg/day for adults [16] and due to its very good biocompatibility it has been proposed to use it alone or as main element in alloys. The main advantage of Zn alloy over Mg alloy and Fe, is its corrosion resistance in body fluid environment, which is intermediate between Fe and Mg [19]. Mostaed et al. studied Zn-Mg and Zn-Al alloys for biodegradable application, in particular for cardiovascular stents [19]. They investigate Zn alloys behaviour in terms of mechanical properties, corrosion resistance and laser interaction, in fact Zn-0.5Mg texture orientation remained unchanged after laser processing, proving the viability in producing Zn-alloys stents [20].

Despite promising results in terms of biological and corrosion performance, a common limitation for the biodegradable metals remains as the increased complexity in the manufacturing of the device. Conventionally, stents are produced from tubular feedstock by laser microcutting. Chemical and electrochemical finishing steps follow and an annealing stage can be incorporated. Such route is well-established and relatively less complex for the conventional stent material AISI 316L stainless steel. An austenitic steel with good formability, chemical stability, and heat resistance renders it suitable for tube drawing, laser microcutting, and chemical polishing processes [21]–[26]. On the other hand, the advantageous properties of both Mg- and Zn-alloys for biodegradability render them poor for processability. The low melting and vaporization points are problematic for laser processing and chemical polishing is highly complex due to the intrinsic low corrosion resistance[27]–[29]. The tubular feedstock requires extrusion and tube drawing processes in order to achieve the tight tolerances required [30]–[33]. A distinction can be made between the biodegradable metals for their formability, where Mg and its alloys are characterized by poorer performance compared to Fe- and Zn-alloys. For all types of materials, the production of minitubes is a complex and costly procedure, especially at a prototyping stage. Sheet material is relatively easier to produce, where dedicated dies are not commonly

required. From this point of view, Zn and its alloys are also preferable due to lower melting point, and lower reactivity compared to the Mg-alloys.

The use of sheet material as a feedstock for testing new biodegradable alloys is an appealing feature. The use of an adequate mesh can also provide the means for expanding the 2D mesh to a 3D tubular structure. Takahata and Gianchandani proposed a planar stent mesh which could be realized by micro EDM on sheet metal and could be expanded in to a cylindrical form [34]. Such designs are appealing for producing functional test devices starting from sheet precursors that enable a faster and easier production route [35]. The use of such geometries can accommodate several types of manufacturing processes in the production route. Laser microcutting is intrinsically a viable process for the production of flat stents. Following the standard route at the prototyping stage with sheet material provides the advantage of developing the process for future mass production employing tubular precursors. The feasibility of such route employing laser microcutting and chemical etching has been demonstrated on a conventional permanent alloy, AISI 316L stainless steel [36]. Indeed both laser microcutting and chemical etching of stainless steel are established processes [8]. However, the possibility to realize the fine flat mesh and consecutively expand it has been the main concern of the previous study. In the light of the positive results, it was possible to use this platform for developing the laser microcutting and chemical etching of a novel biodegradable material namely pure Zn.

Therefore, this work aims to prototype biodegradable stents in Zn following the conventional production route combined with an expandable flat geometry. Initially, the processability of pure Zn is with a ns-pulsed fiber laser is investigated. Chemical etching is applied as a finishing step on the material with an intrinsically high corrosion rate. The prototype stents were expanded with a conventional ballooned catheter as a functional mechanical test.

2. Production route

The production route consisted in the use of sheet material, laser microcutting and chemical etching. In particular, the mesh design allowed for the expansion of the device from a flat configuration to a 3D tubular one. For the expansion, the flat mesh is placed over the catheter over the balloon in an alternating way below and above the struts as shown in Figure 1.a. The tubular structure is retained upon complete inflation of the tube.

For such expansion strategy, the design of Takahata and Gianchandani has been adapted. The original mesh design was produced through micro EDM (electric discharge machining) from stainless steel foils, where the tool size determines the edge radii [34]. The mesh was adapted to laser microcutting as shown in Figure 2.a. Using the micro EDM technology, the process resolution is limited to the tool radius, which is commonly much larger than the kerf width achievable by laser cutting. The control of edge radius is constrained to the tool trajectory, causing sharp edges or very large radii. The use of the focused laser beam allows for achieving kerf widths in the order of 10-30 μm, thus a greater flexibility in the final geometry. The design of Takahata

and Gianchandani was adapted to the laser microcutting technology (see Figure 1.b). Corner radii were increased from 0 µm to 150 µm and horizontal struts were thickened from 50 µm to 100 µm. This modified design consists of a final length of 11 mm with the presence of many scrap parts. Destruction cuts, which are common to miniature tube cutting for stent manufacturing, were introduced to reduce scrap part size and provide an easier detachment from the stent mesh.

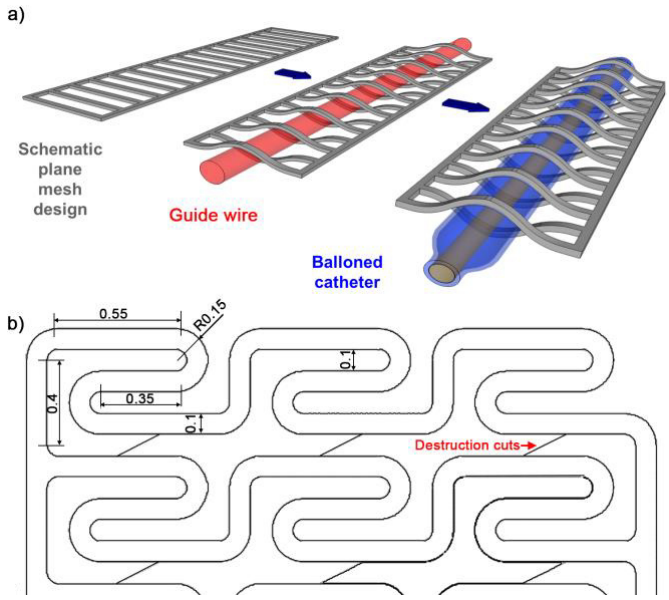

Figure 1. a) Schematic representation of the stent expansion with a planar mesh. b) Stent design for flat to tubular form expansion.

3. Material & Methods

3.1. Material

Pure zinc sheets (99.99% wt Zn) were used for the experimentation. The material was cold rolled to 0.12 mm thickness. Thermal and physical properties of pure Zn are compared to the conventional permanent and biodegradable metal counterparts AISI 316L and AZ31 in

Table **1**. It can be seen that the material properties of Zn render the material prone to increased amount of vaporization during the process.

Table 1 Thermal properties of pure Zn, AISI 316L, and AZ31 [37].

Property	**Symbol**	**Pure Zinc**	**AISI 316L**	**AZ31**
Density	ρ (kg/m$_3$)	7133	8000	1770
Heat Capacity	c_p (J/kg°C)	382	500	1020
Melting point	T_m (K)	693	1723	905
Vaporization Point	T_v (K)	1179	3273	1363
Thermal conductivity	K (W/m·K)	113	21.5	96
Oxidation enthalpy	ΔH (kJ/mol)	-343	-260(Fe)	-602 (Mg)
Viscosity at T_m	η (mPa s)	2.65	6	1.25
Heat diffusivity	α (m$_2$/s)	4.3e-5	0.54e-5	5.32e-5
Latent heat of fusion	L_f(KJ/Kg)	101	260	340
Latent heat of vaporization	L_v (KJ/Kg)	1782	6500	3090

3.2. Laser microcutting system

The employed laser source was a Q-switched pulsed active fiber laser (IPG YLP-1/100/50/50, Cambridge, MA, USA). The laser emitted at 1064 central wavelength, producing pulse repetition rates between 20-80 kHz and pulse durations of 250 ns. The main characteristics of the laser source are summarized in Table **2**. Downstream, the laser source is coupled to a micromachining head (µ Laser Processing Head, HighYAG, Kleinmachnow, Germany) with a 50-mm focal lens and 0.5 diameter nozzle for process gas addition. Using this optical configuration, a calculated 19 µm beam diameter was obtained at the focal point. For positioning, linear axes with air bearings was used (Aerotech ALS-130, Pittsburgh, USA). Metal sheets were positioned in a mask that blocks the piece, on the moving stage of the laser system, that is connected to axis system and permits the moving in x and y direction. Complete set up system is shown in Figure 2.

Table 2 Main characteristics of the employed laser system.

Parameter	Symbol	Value
Laser wavelength	λ	1064 nm
Pulse duration	τ	250 ns
Pulse repetition rate	PRR	20-80 kHz
Maximum average power	$P_{avg,max}$	50 W
Pulse energy	E	0.1-1.2 mJ
Beam quality factor	M_2	1.7
Focused beam diameter	d_0	19 µm

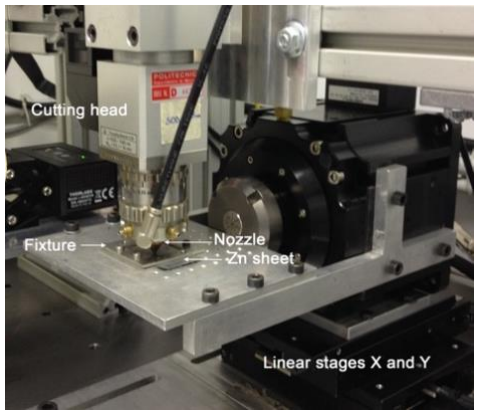

Figure 2. Laser microcutting system configuration.

3.3. Experimental procedure

3.3.1. Material processability window

Given the novelty of the material and the scarcity of information available regarding its processability by laser microcutting, the feasibility window was sought at an initial stage. For this purpose, the main process parameters, which are shown to be among the most influential parameters for the process namely, average power, cutting speed, and process gas were varied in a wide range. Average power was varied between 3 and

22 W, while the cutting speed range was between 1 and 8 mm/s. Shield gas type was varied between N_2 and Ar, whereas 7 bar pressure was fixed for both. The pulse repetition rate was fixed at 35 kHz. A stand-off distance of 0.2 mm was employed and the focal position was fixed at the sample surface. Scanning electron microscopy (SEM, Zeiss EVO 50, Oberkochen, Germany) was used to investigate the samples surface morphology at high magnification. The results were analysed categorically in terms of cut quality.

3.3.2. Dross formation investigation

At a second stage, the conditions within the feasibility window were further analysed by employing quantitative measurements. In particular, the top side of the cut kerf was examined with the aim to measure the dross area (A_{dross}). An image processing software was used for the purpose as shown in Figure 3 measuring the dross area on 220 µm cut length. The feasible condition for the production of the flat stent mesh was determined by the end of this characterization. For the chosen condition, cross-section was taken to further analyse the kerf width at the entrance and at the exit of the kerf employing optical microscopy (Leitz Ergolux 200, Leica, Wetzlar, Germany). Experimental conditions for laser micro-cutting are summarized in Table 3.

Table 3 Fixed and varied parameters in the laser microcutting experiments.

Fixed parameters	
Pulse repetition rate, PRR (kHz)	35
Process gas pressure (bar)	7
Focal position, Δz (mm)	0
Stand-off distance, SOD (mm)	0.2
Varied parameter	
Average power, P_{avg} (W)	3-22
Cutting speed, v (mm/s)	1-8
Process gas type	Ar, N_2

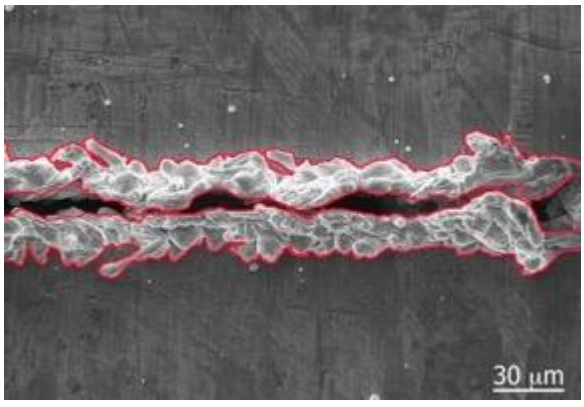

Figure 3 Example of a dross area measurement.

3.3.3. Chemical etching

Chemical etching was studied for the chosen laser microcutting condition for producing the stent mesh only. The etching process was applied at room temperature, and after immersion in the etching solution, the samples were rinsed with water and then dried in ambient air. Each set of samples was etched in 50 mL of fresh etchant.

Two aqueous etchants were employed for the study. Solution 1 consisted of 5 mL HNO_3 and 100 mL H_2O. Solution 2 was weaker variant of Solution 1 with 2.5 mL HNO_3. Square shaped specimens with 2x2 mm^2 size were cut with the chosen laser microcutting parameters were immersed with variable durations of 10, 20, 30, and 40 seconds. Dross removal was investigated. observed through optical microscopy (Lecia Leitz Ergolux 200, Wetzlar, Germany). SEM images were taken to investigate the morphological changes before and after chemical etching (Zeiss EVO 50, Oberkochen, Germany). Thickness variation was measured by a linear measurement machine (Microrep Joint Instruments DMS 680, Milan, Italy). The reduction in thickness (Δr) was calculated using the following expression:

$$\Delta r = \frac{t_f - t_i}{t_i} \cdot 100 \quad (1)$$

where t_i and t_f are the initial thickness and the thickness after the chemical etching process respectively. Focus variation microscopy (Alicona Infinite Focus, Graz, Austria) was used to measure the surface roughness parameters (Ra, Rq, and Rz) before and after chemical etching. The parameters of the experimental conditions are summarized in Table 4.

Table 4 Fixed and varied parameters in the chemical etching of pure Zn.

Fixed parameters	
Temperature, (°)	20
Varied parameter	
Etchant type	Solution 1: 5 mL HNO_3 +100 mL H_2O Solution 2: 2.5 mL HNO_3 + 100 mL H_2O
Etching duration (s)	10, 20, 30, 40

4. Results

4.1. Zn feasibility window

The visual inspection over the cut kerfs showed distinct cutting conditions as function of process parameters. The cut kerf quality varied strongly as a function of average power. In particular, four classes were identified as: *Uncut, Limit condition, Cut, Irregular cut*. Example images of each condition are reported in Figure 4. The *Uncut* is characterised by an incomplete penetration of the cut, as the bottom of the kerf is closed. By increasing power levels, a partially opened kerf is viewed. Both for *Uncut* and *Limit condition*, the dross is mainly composed of molten deposits around the kerf. In *Limit condition* a small fraction of vapour deposits in form of micrometric particulate is viewed. The *Cut* condition is characterized by an open kerf, increased fraction of condensed vapour droplets and dross formation also around the bottom side of the kerf. The dross on the top side of the kerf appears to be fragmented, showing signs of a rapid cooling cycle. At higher laser power levels, *Irregular cut* is observed. The kerf width expands irregularly forming large droplets of molten material. Such conditions are not acceptable for the maintaining the precision required for the application.

Figure 5 reports the distribution of the quality classes as a function of process parameters. It can be observed that the class change is mainly induced by the laser power, while both cutting speed and process gas appear to have no influence. In Figure 5 the feasibility window for both the process gases are indicated. For both of the gases laser power between 5.5 and 12.6 W and the complete cutting speed range between 1 and 8 mm/s were found to be adequate. This implies that for processability purposes the use of a more expensive inert gas such as Ar is not required.

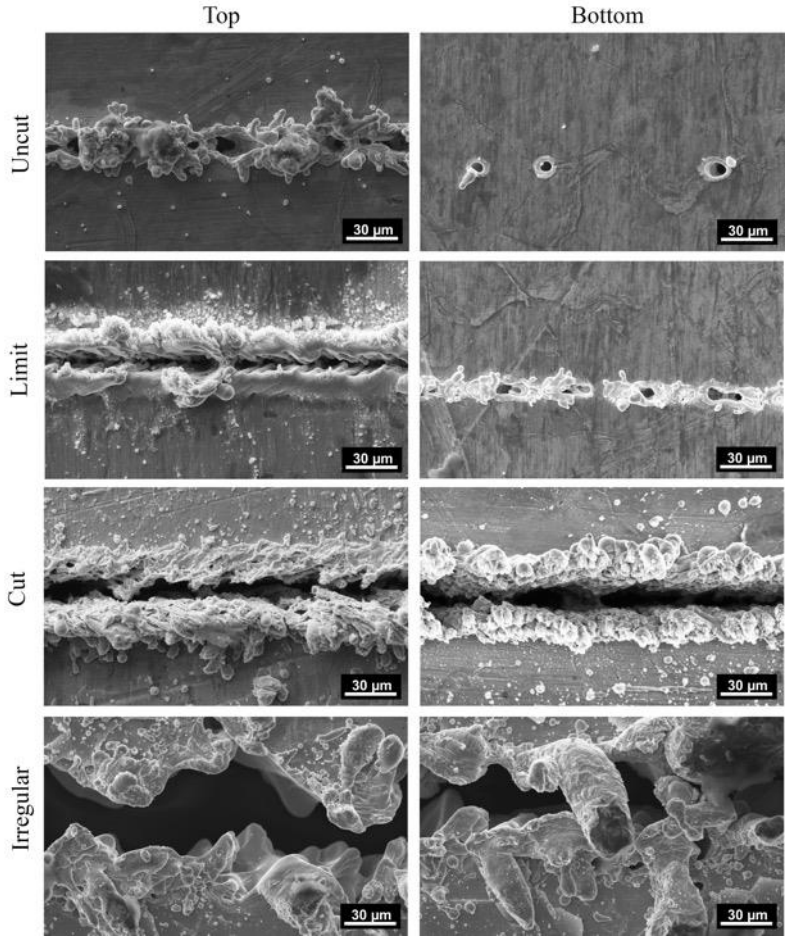

Figure 4 Different quality classes observed in the laser microcutting study.

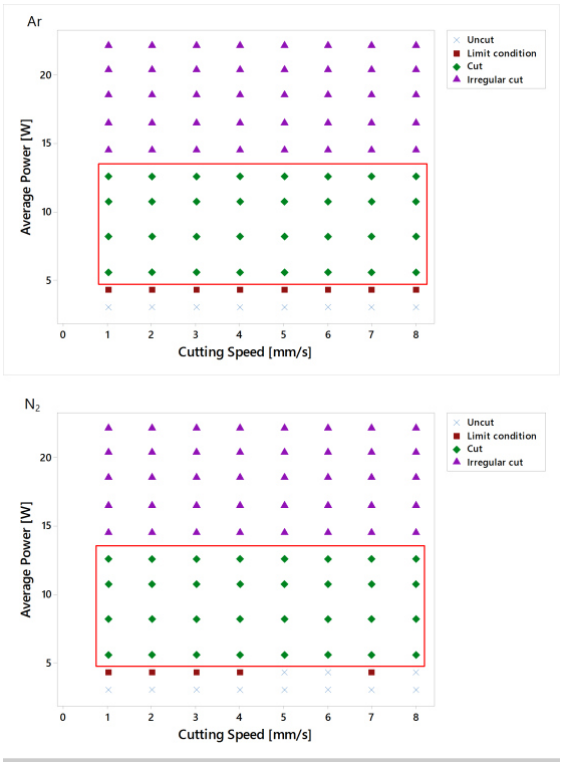

Figure 5 Feasibility window of pure Zn sheet laser cutting with Ar (a) and N2 (b).

4.2. Dross formation analysis

Further investigations were carried out in terms of the dross quantity. In Figure 6 is shown the trend of the dross area of pure zinc kerf within the feasibility window as a function of assistance gas, cutting speed and power. Curves show an asymptotic behaviour as a function of cutting speed. The main influential parameter is the average power, which increases the dross area. At higher average power values, N_2 appears to generate a higher amount of dross. The use of Ar may increase the plasma formation, which may contribute to the material removal by vaporizing the dross around the cut kerf. As a compromise between production cost and quality, processing conditions were determined as summarized in Table 5. Process gas was fixed as N_2, whereas average power was fixed at 8.1 W and cutting speed was 2 mm/s. Figure 7 shows the geometrical characteristics of the cut kerf obtained using the selected parameters.

Table 5 Laser cutting parameter optimized for stent microcutting.

Parameter	Value
Average power, P_{avg}	8.1 W
Pulse repetition rate, PRR	35 kHz
Cutting speed, v	2 mm/s
Focal position, Δz	0 mm
Stand-off distance, SOD	0.2 mm
Process gas type	N_2
Process gas pressure	7 bar

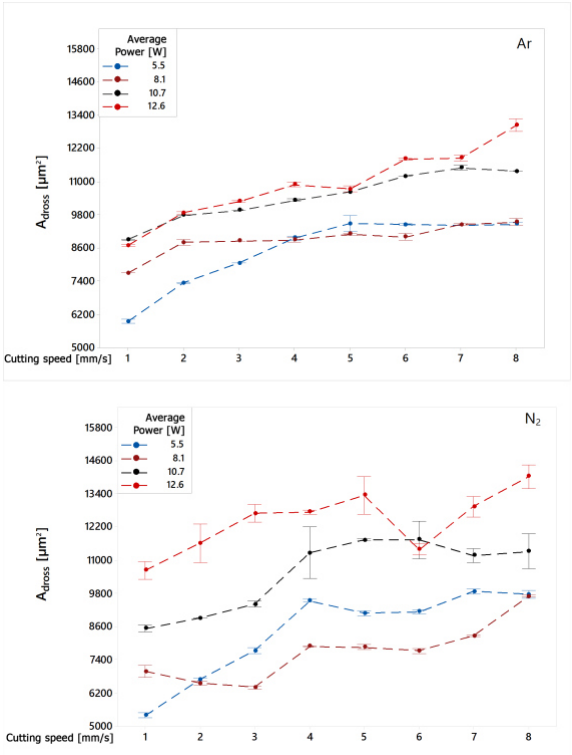

Figure 6 Dross area as a function of process gas, speed and power. Error bars represent standard deviation. Dashed lines are to depict trend only.

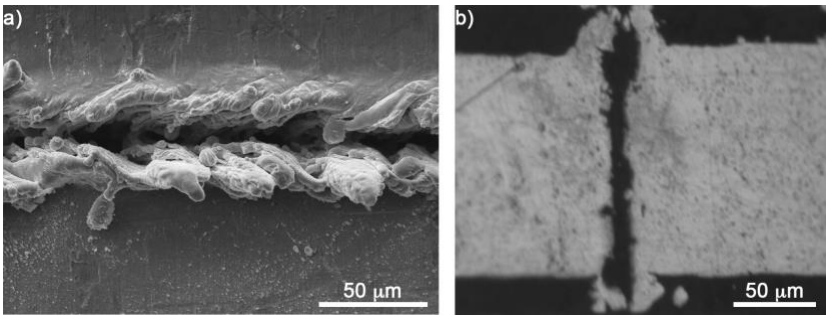

Figure 7 SEM image (a) and optical image (b) of optimized kerf cut.

The pure Zn shows distinct conditions in terms of processability by laser microcutting. As a comparison, other metallic alloys used for stent manufacturing can be taken into account. AISI 316L stainless steel requires the use of O_2 as the reactive process gas, which provides further energy into the process due to the oxidation process [8]. The resultant dross is highly oxidised and selectively removable by chemical etching providing a high final quality. On the other hand, the biodegradable AZ31 Mg alloy is processed using Ar and relatively low laser power levels [10]. It can be expected that pure Zn is prone to generate high amount of dross and vapour due to very low melting and vaporization temperature. The dross amount after laser cutting plays a critical role on the final quality achievable by the end of the finishing process [38]. A common approach in macro laser cutting is to manage the gas flow in terms of pressure and nozzle design [39]. The delicate nature of the thin sheet materials and microtubes is a restriction on the applicability of high pressure, which would deform the workpiece. From this perspective, the use of ultrashort fs- to ps-long pulses can reduce the dross

formation by avoiding heat generation within the process. Submerged cutting can be also explored in order to dissolve the dross during the laser microcutting operation [27].

4.3. Chemical etching analysis

Figure 8 represents the thickness reduction as a function of chemical etching conditions. It can be seen that the higher amount of HNO_3 and prolonged durations of etching induce a reduction of up to 6%. The solution composed by 2.5% HNO_3 applied for 30 seconds was chosen observed to be effective in removing the surface dross, whereas further immersion did not provide any notable improvement. Providing also less than 2% thickness reduction in average, this condition was chosen for stent production.

Figure 9 depicts the SEM images of the kerf profiles before and after chemical etching, showing a clear improvement of surface quality both in terms the removal of the dross and reduction of the roughness. Focus variation microscopy images are reported in Figure 10, whereas the relative surface roughness measurements are shown in Figure 11. Chemical etching provides an average of 47% decrease in average roughness (Ra), whereas the Rz value is decreased by 57% in average. The process provides a clean kerf removing the recast and dross and leaving out a smoother surface. Further electrochemical polishing should be studied for reducing the surface roughness to the implantation requirements.

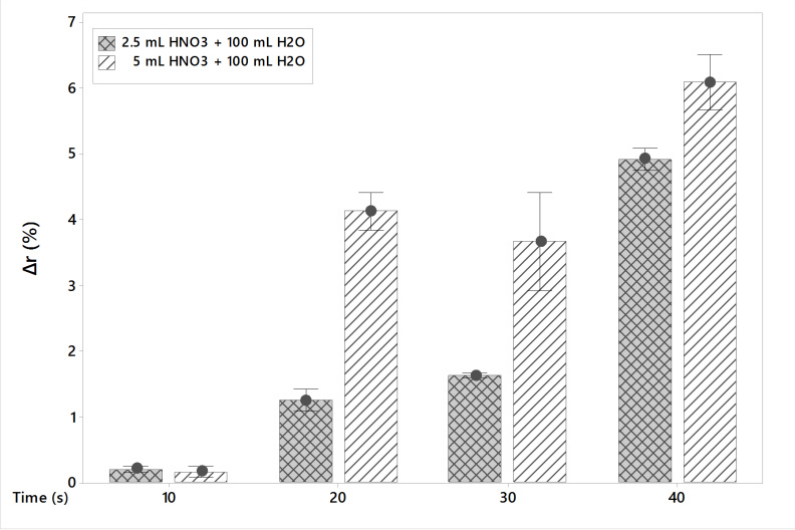

Figure 8 Evolution of thickness reduction as a function of time and chemical etching solution. Error bars represent standard deviation.

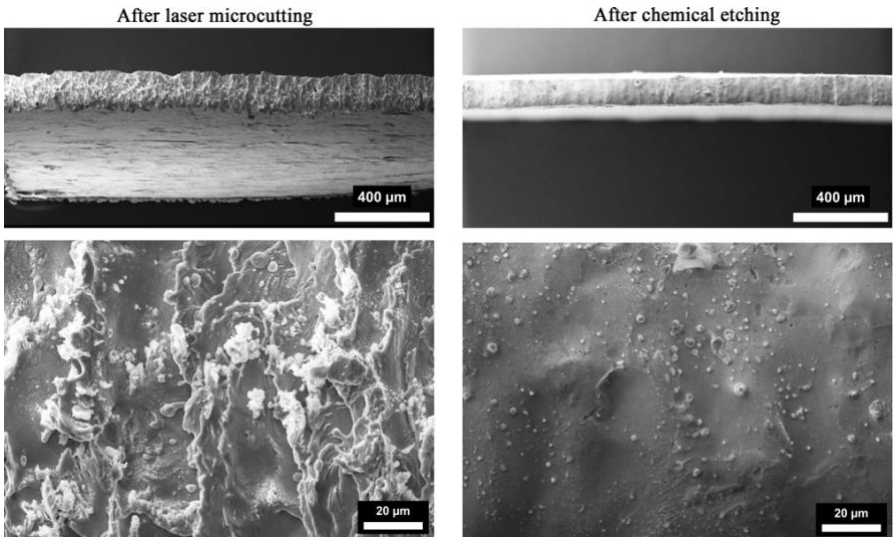

Figure 9 SEM images of the cut kerf after laser cutting (P_{avg}= 8.1 W, v= 2 mm/s, N_2 at 7 bar) and after consecutive chemical etching (2.5% HNO_3 + 100 mL H_2O for 30 seconds).

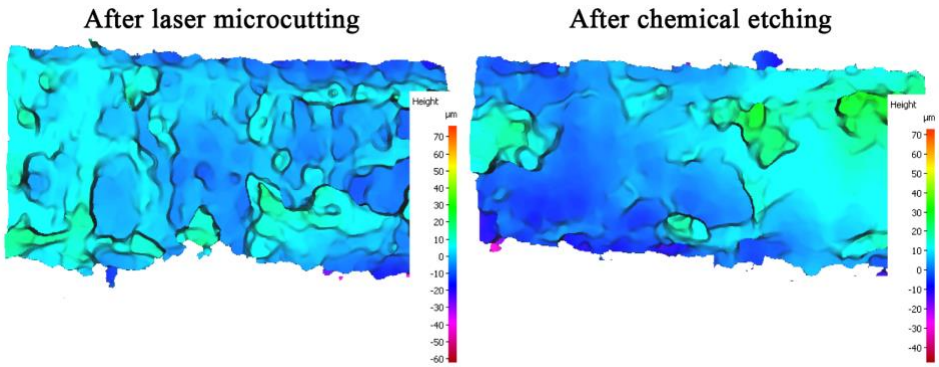

Figure 10 Focus variation microscopy images of kerf profiles after laser cutting and after chemical etching.

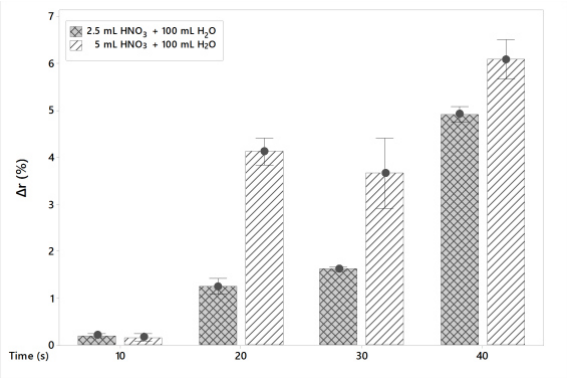

Figure 11 Surface roughness variation at different stages of the stent manufacturing cycle.

4.4. Prototyping of flat stents

Prototype flat stents were produced following the production route determined in the experimental phases. SEM images of the prototype stents at different stages of production are shown in **Figure 12**. As common to

laser microcutting using ns-pulsed lasers, the cut mesh remained attached to the scrap parts by the end of the process due to the unclean kerf. Chemical etching provided the separation of almost all the scrap part, leaving out an improved surface quality. However, due to the complex mesh geometry the efficacy of the chemical etching step may be reduced. This is also due to the fact that the etchant does not effectively reach the cut kerf due to the scrap parts. However, high geometrical fidelity has been observed at these stages. For the final detachment of the scrap parts, the stents were further cleaned in an ultrasonic bath immersed in acetone for 5 minutes. As a result, complete scrap removal and further dross detachment could be achieved without excessively reducing the strut thickness.

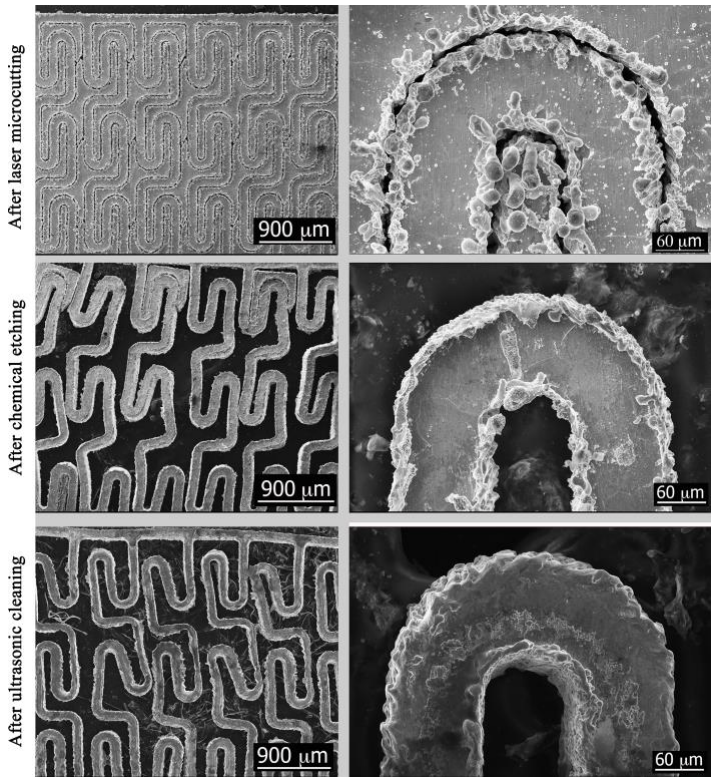

Figure 12 Pure Zn stents after laser microcutting, chemical etching, and ultrasonic cleaning phases.

After the successful production of the flat mesh, the produced prototypes were mounted on a ballooned catheter system with maximum diameter of 2.5mm, were pressed to return to flat configuration and were deployed with pressure up to 15 bar using syringe equipped with manometer. Pressure required to expand pure Zn stent was about 6 bar. As shown in Figure 13, the pure Zn could be expanded to a tubular form. The surface appears smooth and clean, confirming efficacy of laser cutting and chemical etching and above all the expandability of the stent. The expansion stage also serves as a function mechanical test both for the alloy type, which can be carried out as a comparative manner at this exploratory stage. Due to its very poor mechanical properties, pure Zn prototypes did not withstand the deployment stage, whereas the same mesh has been proven to function on AISI 316L and AZ31[40].

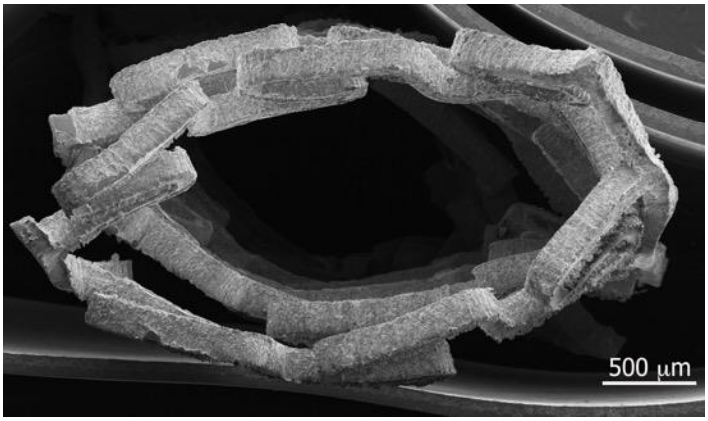

Figure 13 Flat stent prototype in biodegradable pure Zn after expansion.

5. Conclusions

This work presented the prototyping of biodegradable pure Zn stents using the conventional production route based on laser microcutting and chemical etching, employing a planar stent mesh. The work has tackled the different issues related to the design modifications to the processing requirements, providing several insights to the manufacturing of future biodegradable stents in Zn-alloys

The research outcomes can be summarized as follows:

- Pure Zn shows different processing conditions as a function of average power and cutting speed. In particular, at high average power levels the process reaches a distinct irregular cutting region, where excessive dross is generated and kerf geometry is no longer acceptable for high precision laser microcutting applications.
- Pure Zn resists well to the chemical etching phase with aqueous HNO_3 solutions, where thickness reduction is limited to less than 10% upon effective dross removal.
- The complex mesh geometry renders the etching process more difficult. Hence it is advisable to use ultrasonication without the use of an etchant for complete scrap and dross removal due to the mechanical action.
- The planar meshes could be successfully expanded using a commercial biomedical catheter. The expansion stage acts also as a mechanical test depicting the strength of the alloy and the mesh. This mesh can be used as a comparative platform not only for mechanical purposes but also to evaluate the biomedical performance.

Despite providing a complete view over the production route of prototype biodegradable stents in pure Zn, this work leaves out open questions for future assignments. Planar stents are still a long way to come and many experimental steps are necessary to prove the reliability of these devices. Electropolishing of Zn-alloys requires further investigation. In-vivo and in-vitro tests should be carried out to identify the final biological performance of the device.

References

[1] A. G. Demir, B. Previtali, Q. Ge, M. Vedani, W. Wu, F. Migliavacca, L. Petrini, C. A. Biffi, and M. Bestetti, "Biodegradable magnesium coronary stents: material, design and fabrication," *Int. J. Comput. Integr. Manuf.*, vol. 27, no. 10, pp. 936–945, 2014.

[2] D. Stoeckel, C. Bonsignore, S. Duda, and M. Dunitz, "A survey of stent designs.," *Minim. Invasive Ther. Allied Technol.*, vol. 11, no. 4, pp. 137–47, Jul. 2002.

[3] N. S. Murni, M. S. Dambatta, S. K. Yeap, G. R. A. Froemming, and H. Hermawan, "Cytotoxicity evaluation of biodegradable Zn-3Mg alloy toward normal human osteoblast cells," *Mater. Sci. Eng. C*, vol. 49, pp. 560–566, 2015.

[4] H. Hermawan, D. Dubé, and D. Mantovani, "Developments in metallic biodegradable stents.," *Acta Biomater.*, vol. 6, no. 5, pp. 1693–7, May 2010.

[5] M. I. Ther, A. Technol, D. Stoeckel, C. Bonsignore, and S. Duda, "A Survey of Stent D . signs," *Cell*, 2002.

[6] A. Purnama, H. Hermawan, and D. Mantovani, "Biodegradable Metal Stents: A Focused Review on Materials and Clinical Studies," *J. Biomater. Tissue Eng.*, vol. 4, no. 11, pp. 868–874, 2014.

[7] G. L. Song and A. Atrens, "Corrosion Mechanisms of Magnesium Alloys," *Adv. Eng. Mater.*, vol. 1, no. 1, pp. 11–33, 1999.

[8] A. G. Demir, B. Previtali, D. Colombo, Q. Ge, M. Vedani, L. Petrini, W. Wu, and C. A. Biffi, "Fiber laser micromachining of magnesium alloy tubes for biocompatible and biodegradable cardiovascular stents," in *Progress in Biomedical Optics and Imaging - Proceedings of SPIE*, 2012, vol. 8237.

[9] F. Witte, N. Hort, C. Vogt, S. Cohen, K. U. Kainer, R. Willumeit, and F. Feyerabend, "Degradable biomaterials based on magnesium corrosion," *Curr. Opin. Solid State Mater. Sci.*, vol. 12, no. 5–6, pp. 63–72, 2008.

[10] A. G. Demir, B. Previtali, and C. A. Biffi, "Fibre Laser Cutting and Chemical Etching of AZ31 for Manufacturing Biodegradable Stents," *Adv. Mater. Sci. Eng.*, vol. 2013, pp. 1–11, 2013.

[11] Y. P. Kathuria, "The potential of biocompatible metallic stents and preventing restenosis," *Mater. Sci. Eng. A*, vol. 417, no. 1–2, pp. 40–48, 2006.

[12] F. Witte, V. Kaese, H. Haferkamp, E. Switzer, A. Meyer-Lindenberg, C. J. Wirth, and H. Windhagen, "In vivo corrosion of four magnesium alloys and the associated bone response," *Biomaterials*, vol. 26, no. 17, pp. 3557–3563, 2005.

[13] G. Manivasagam, D. Dhinasekaran, and A. Rajamanickam, "Biomedical Implants: Corrosion and its Prevention - A Review," *Recent Patents Corros. Sci.*, vol. 2, no. 1, pp. 40–54, Jun. 2010.

[14] M. Peuster, C. Hesse, T. Schloo, C. Fink, P. Beerbaum, and C. von Schnakenburg, "Long-term biocompatibility of a corrodible peripheral iron stent in the porcine descending aorta," *Biomaterials*, vol. 27, no. 28, pp. 4955–4962, 2006.

[15] H. Hermawan, A. Purnama, D. Dube, J. Couet, and D. Mantovani, "Fe-Mn alloys for metallic biodegradable stents: Degradation and cell viability studies," *Acta Biomater.*, vol. 6, no. 5, pp. 1852–1860, 2010.

[16] P. K. Bowen, J. Drelich, and J. Goldman, "Zinc exhibits ideal physiological corrosion behavior for bioabsorbable stents," *Adv. Mater.*, vol. 25, no. 18, pp. 2577–2582, 2013.

[17] J. G. Gong, H., Wang, K., Strich, R., Zhou, "In vitro biodegra- dation behavior, mechanical properties, and cytotoxicity of biodegradable Zn–Mg alloy," *7th Symp. Biodegrad. Met. Abstr. B.*, 2015.

[18] D. Vojtěch, J. Kubásek, J. Šerák, and P. Novák, "Mechanical and corrosion properties of newly developed biodegradable Zn-based alloys for bone fixation," *Acta Biomater.*, vol. 7, no. 9, pp. 3515–3522, 2011.

[19] J. Cheng, B. Liu, Y. H. Wu, and Y. F. Zheng, "Comparative invitro study on pure metals (Fe, Mn, Mg, Zn and W) as biodegradable metals," *J. Mater. Sci. Technol.*, vol. 29, no. 7, pp. 619–627, 2013.

[20] "Novel Zn-based alloys for biodegradable stent applications: Design, Development and In Vitro Degradation."

[21] Y. P. Kathuria, "Laser microprocessing of metallic stent for medical therapy," *J. Mater. Process. Technol.*, vol. 170, no. 3, pp. 545–550, Dec. 2005.

[22] H. Meng, J. Liao, Y. Zhou, and Q. Zhang, "Laser micro-processing of cardiovascular stent with fiber laser cutting system," *Opt. Laser Technol.*, vol. 41, no. 3, pp. 300–302, 2009.

[23] K. Kleine, B. Whitney, and K. Watkins, "Use of fiber lasers for micro cutting applications in the

medical device industry," *Icaleo*, vol. 2002, no. Icaleo, pp. 1–11, 2002.
[24] C. Momma, U. Knop, and S. Nolte, "Laser cutting of slotted tube coronary stents—state-of-the-art and future developments," *Prog. Biomed. Res.*, vol. 4, no. February, pp. 39–44, 1999.
[25] J. Lu, R. Q. Xu, X. Chen, Z. H. Shen, X. W. Ni, S. Y. Zhang, and C. M. Gao, "Mechanisms of laser drilling of metal plates underwater," *J. Appl. Phys.*, vol. 95, no. 8, pp. 3890–3894, 2004.
[26] N. Muhammad, D. Whitehead, a. Boor, and L. Li, "Comparison of dry and wet fibre laser profile cutting of thin 316L stainless steel tubes for medical device applications," *J. Mater. Process. Technol.*, vol. 210, no. 15, pp. 2261–2267, Nov. 2010.
[27] A. G. Demir and B. Previtali, "Dross-free submerged laser cutting of AZ31 Mg alloy for biodegradable stents," *J. Laser Appl.*, vol. 28, no. 3, 2016.
[28] M. Montani, A. G. Demir, E. Mostaed, M. Vedani, and B. Previtali, "Processability of pure Zn and pure Fe by SLM for biodegradable metallic implant manufacturing," *Rapid Prototyp. J.*, vol. 23, no. 3, 2017.
[29] A. G. Demir, L. Monguzzi, and B. Previtali, "Selective laser melting of pure Zn with high density for biodegradable implant manufacturing," *Addit. Manuf.*, vol. 15, 2017.
[30] Q. Ge, M. Vedani, and G. Vimercati, "Extrusion of magnesium tubes for biodegradable stent precursors," *Mater. Manuf. Process.*, vol. 27, no. 2, pp. 140–146, 2012.
[31] S. H. Hsiang and Y. W. Lin, "Investigation of the influence of process parameters on hot extrusion of magnesium alloy tubes," *J. Mater. Process. Technol.*, vol. 192–193, pp. 292–299, 2007.
[32] D. L. Atwell and M. R. Barnett, "Extrusion limits of magnesium alloys," *Metall. Mater. Trans. A Phys. Metall. Mater. Sci.*, vol. 38 A, no. 12, pp. 3032–3041, 2007.
[33] Q. Ge, D. Dellasega, A. G. Demir, and M. Vedani, "The processing of ultrafine-grained Mg tubes for biodegradable stents.," *Acta Biomater.*, vol. 9, no. 10, pp. 8604–10, Nov. 2013.
[34] K. Takahata and Y. B. Gianchandani, "A planar approach for manufacturing cardiac stents: Design, fabrication, and mechanical evaluation," *J. Microelectromechanical Syst.*, vol. 13, no. 6, pp. 933–939, 2004.
[35] S. C. Gott, B. A. Jabola, and M. P. Rao, "Vascular stents with submicrometer-scale surface patterning realized via titanium deep reactive ion etching," *J. Micromechanics Microengineering*, vol. 25, no. 8, p. 085016, 2015.
[36] G. Catalano, A. G. Demir, V. Furlan, and B. Previtali, "Use of Sheet Material for Rapid Prototyping of Cardiovascular Stents," in *Procedia Engineering*, 2017, vol. 183.
[37] "ASM Handbook, American Society for Metals, Metals Park, http://products.asminternational.org/hbk/index.jsp, 2013," p. 2013, 2013.
[38] A. G. Demir and B. Previtali, "Comparative study of CW, nanosecond- and femtosecond-pulsed laser microcutting of AZ31 magnesium alloy stents," *Biointerphases*, vol. 9, no. 2, p. 029004, 2014.
[39] M. Anilli, A. G. Demir, and B. Previtali, "Additive manufacturing of laser cutting nozzles by SLM: processing, finishing and functional characterization," *Rapid Prototyp. J.*, vol. 24, no. 3, 2018.
[40] G. Catalano, A. G. Demir, V. Furlan, and B. Previtali, "Laser microcutting of sheet metal for prototyping expandable stent-like structures in permanent and biodegradable alloys," in *RTSI 2017 - IEEE 3rd International Forum on Research and Technologies for Society and Industry, Conference Proceedings*, 2017.